Stability and Quench Behavior of $YBa_2Cu_3O_{7-x}$ Coated Conductor at 4.2 K, Self-Field

Honghai Song, *Student Member, IEEE* and Justin Schwartz, *Fellow, IEEE*

***Abstract*—$YBa_2Cu_3O_{7-x}$ (YBCO) coated conductors (CCs) are now capable of carrying very high transport critical current density J_c over a broad range of magnetic field and temperature space, and as a result, they are receiving significant interest for a wide range of applications. While many of these applications take advantage of the high-temperature performance of YBCO CCs, because the YBCO CC is typically produced on a high-strength substrate and carries very high J_c at very high magnetic field, there is now growing interest in using YBCO CCs at 4.2 K to generate very high magnetic fields. The transition from high-field conductor to high-field superconducting magnet, however, requires that some challenging issues be addressed. One of the most important challenges remaining is to better understand the stability and quench behavior at 4.2 K, so that an effective quench protection system can be developed. Here, we report on measurements of the stability and quench behavior of short YBCO CC at 4.2 K by inducing a quench via a heat pulse from a heater mounted on the conductor surface. Through gradually increasing heater pulse amplitude, the transition from stable to unstable (i.e., recovery to quench) is observed through voltage and temperature measurements. Using these data, the minimum quench energy (MQE) and normal zone propagation velocity (NZPV) are determined. It is found that, for the same fraction of critical current (I/I_c), YBCO CCs have similar MQE and NZPV as Ag-alloy-clad $Bi_2Sr_2CaCu_2O_x$ wires and significantly higher MQE and lower NZPV than those of MgB_2 round wires of similar I_c (4.2 K). Furthermore, the voltage and temperature versus time data are correlated to better understand the quench onset behavior at 4.2 K. It is determined that a normal temperature gradient exists from the CC surface to the YBCO layer within the conductor, as well as a directly measured longitudinal temperature gradient. After the heater pulse has ended but while the transport current continues, the temperature gradient along the length becomes dominant. Nevertheless, voltage and temperature measurements remain problematic for quench detection in large magnets because of the slow longitudinal propagation velocity. Thus, new approaches to quench detection and/or protection of high-field YBCO magnets are needed. PACS number(s): 84.71. Mn**

***Index Terms*—Coated conductor (CC), stability and quench, $YBa_2Cu_3O_{7-x}$ (YBCO), 4.2 K.**

Manuscript received February 11, 2009; revised May 4, 2009. This paper was recommended by Associate Editor P. J. Masson. This work was supported in part by the Air Force Office of Scientific Research and in part by the U.S. Department of Energy.

H. Song is with the Applied Superconductivity Center, National High Magnetic Field Laboratory, and the Department of Electrical and Computer Engineering, FAMU-FSU College of Engineering, Florida State University, Tallahassee, FL 32310 USA.

J. Schwartz is with the Applied Superconductivity Center, National High Magnetic Field Laboratory, and the Department of Mechanical Engineering, FAMU-FSU College of Engineering, Florida State University, Tallahassee, FL 32310 USA.

Color versions of one or more of the figures in this paper are available online at http://ieeexplore.ieee.org.

Digital Object Identifier 10.1109/TASC.2009.2023674

I. Introduction

THE UTILITY of a superconducting material is determined by its ability to carry a significant critical current density J_c at the temperature and magnetic field required by the application. Due to the fundamental limits on the upper critical field, low-temperature superconductors (LTSs) such as NbTi and Nb_3Sn are not likely to generate magnetic fields greater than about 23 T [1], [2]. High-temperature superconductors (HTSs), however, have upper critical fields that are estimated to be at least 90 T and, therefore, create the possibility for the generation of much higher magnetic fields [3]. Of the HTS conductors that have been developed, the potential for low cost and the demonstrated high J_c in $YBa_2Cu_3O_{7-x}$ (YBCO) coated conductors (CCs) indicate the potential for broad use in a number of applications [4]–[7]. Thus, this technology is being extensively researched [8]–[17]. While the specific details of the commercial CC options vary, they all have certain common features. As implied by their name, CCs are manufactured by coating the superconducting YBCO on a textured substrate, which provides a template for bi-axial texturing in the YBCO layer. The substrate is typically comprised of a Ni-alloy (hastelloy or a Ni-W alloy), upon which one or more oxide buffer layers have been deposited to provide a barrier that prevents chemical interactions between the YBCO and Ni. The top surface of the YBCO layer is protected by a Ag "cap layer," and the entire architecture is then typically encased in Cu or another stabilizer material. There are also a number of options for additives within the YBCO layer that can improve the superconducting properties [18]–[23]. While the details of the electrical transport behavior at high field and the mechanical behavior of the conductor vary with the architecture and processing details, J_c measurements in magnetic fields of at least 25 T clearly show that the behavior at 4.2 K is attractive for high-field magnets [3], [24], [25]. Furthermore, the length scales of commercial YBCO CC manufacturing have significantly increased, and kilometer lengths of YBCO conductor are now available [26], [27]. There has also been significant progress in the application of YBCO CCs to high-field insert magnets, including the recent generation of 26.8 T [26], and dc solenoids generating magnetic fields of as high as 50 T are now being envisioned for nuclear magnetic resonance and muon collider applications [28], [29].

Significant challenges remain before high-field YBCO magnets can be constructed and operated in functional systems [28], [30]. One of the most important challenges is understanding the stability and quench behavior of the YBCO conductor to protect the conductor and magnet from degradation during a

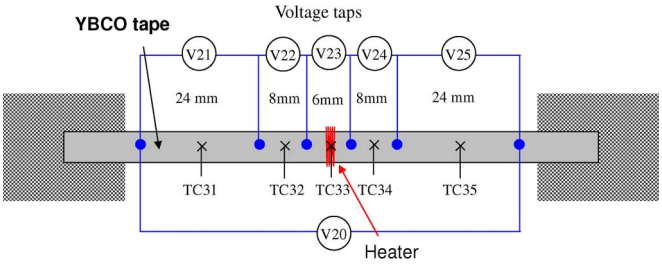

Fig. 1. Schematic of the YBCO CC sample mounted for critical current and quench experiments. Shown are the five voltage pairs (V21–V25) for section voltages and the end-to-end voltage pair V20. Also shown are the five thermocouple locations and naming convention, and the location of the nichrome heater wire, which is wound around the sample. Note that the center thermocouple TC33 is mounted after the heater wire is wound and that the heater wire is electrically insulated and is thus a separate circuit.

quench [3], [24], [31]–[53]. Typically, the minimum quench energy (MQE) and the normal zone propagation velocity (NZPV) are measured to characterize the primary quench behaviors. For YBCO conductors, however, most of the reported quench experiments were performed at temperatures above ∼30 K, yet conductor degradation due to quenching is still not well understood [42], [43], [46]–[50], [53]–[62]. Moreover, the stability and quench of the YBCO conductor with high transport currents at 4.2 K are likely to be significantly different than those at 77 K or under adiabatic conditions (> 30 K). In this paper, the self-field quench behavior of the YBCO CC is explored at 4.2 K, where the conductor is bath-cooled in liquid helium. The transition from recovery to quench is observed by gradually increasing heater pulse voltages, and the MQE and NZPV are reported. The voltage and temperature profiles versus time are evaluated, and finally, the results are compared to those of Bi2212 and MgB_2 at 4.2 K and to the YBCO CC at higher temperature.

II. Experimental Approach

A. CC YBCO Short Sample

A "344" YBCO CC that is ∼4.3 mm wide, 0.22 mm thick, and 12.0 cm long is provided by the American Superconductor Corporation. The conductor, which is described in detail elsewhere, has high I_c through a double-coating technology and engineered flux pinning, which also reduces the electromagnetic anisotropy [24], [63]. After coating, the conductor is slit to a 4-mm width and then laminated with copper stabilizer layers (via soldering) on each side. The Cu strip and, thus, the final conductor architecture are ∼4.3 mm wide.

B. Experimental Setup

An experiment setup for a low-temperature stability test is shown in Fig. 1 [46], [47]. The YBCO sample is soldered to current lead terminals. The conductor is divided into five sections for voltage measurements, i.e., V21, V22, V23, V24, and V25; V20 refers to the end-to-end (ETE) voltage. As shown in Fig. 1, the section lengths are not uniform; rather, they are 24, 8, 6, 8, and 24 mm, respectively. A nichrome (80% Ni and 20% Cr, with 0.203-mm diameter) wire heater is tightly wound around the center section, i.e., V23. The heater, with a wire length of 6.56 cm, has a resistance of 4.37 Ω at 77 K and 4.34 Ω at 4.2 K. After being wound around the center of the conductor, the effective width of the heater area is 4.0 mm. Thus, considering a width of 4.35 mm and a thickness of 0.22 mm, the effective heater volume is 4.79 cm^3. Five type-E thermocouples, i.e., TC31, TC32, TC33, TC34, and TC35, are attached to the conductor surface using GE varnish. The thermocouples are then reglued with Stycast 2850FT (mass ratio of 100 : 7.5) to ensure that they remain attached during 4.2-K experiments. Lastly, the instrumented probe assembly is inserted into a vacuum-jacketed cryostat [64].

To properly plan stability and quench experiments and interpret the results, it is necessary to know the conductor critical current I_c as a function of location. Thus, after inserting the probe into the cryostat, the conductor is cooled in liquid nitrogen to 77 K. The I_c and n value are then measured as a function of location using electric-field criterions of 1 and 0.1 μV/cm. The measurements are then repeated at 40, 27, and 16 K in helium gas during cooling to 4.2 K. I_c is not measured at 4.2 K, because it is expected to approach 1 kA and the sample may be damaged.

C. Experimental Protocol

Stability and quench experiments are performed at 4.2 K in liquid helium. After cooling, transport current I is, first, slowly ramped to some fraction of the ETE I_c and held for 200 ms to ensure that a stable equilibrium is established (HP 6681 System dc power supply). The current is determined from a voltage signal across a shunt resistor (1000 A–100 mV) that is in series with the YBCO CC sample. A heater pulse is then generated by a dc power supply (Kepco BOP 50-4D). The heater energy is varied through the heater pulse magnitude rather than the pulse duration, which is fixed at 300 ms. Typically, a relatively low heat pulse is used in the first run, and it is systematically increased until the conductor quenches. The sample and shunt voltages are measured by an array of digital multimeters (DMMs), except for those across the heater, i.e., V23, V24, and V25, which are recorded by a digital phosphor oscilloscope (Tecktronic TDS 5104) with high resolution at 10 μs/data point. Thermocouple voltages are scanned by an array of four Keithley 2700 DMMs with a sampling rate of 20 ms/data point, including channel switching time. All of the instruments are connected to a personal computer through General Purpose Interface Bus to Universal Serial Bus and controlled by an interactive LabView program. Both software and hardware protection limits are set for turning off the transport current [46], [48], [51].

III. Experimental Results

A. Critical Current and Current-Sharing Temperatures

The 77-K I_c measurements are repeated three times, and the results using a 1-μV/cm electric field criterion are shown in Fig. 2. Note that there is some nonuniformity in the electrical performance (∼10%) along the length. It is possible that the

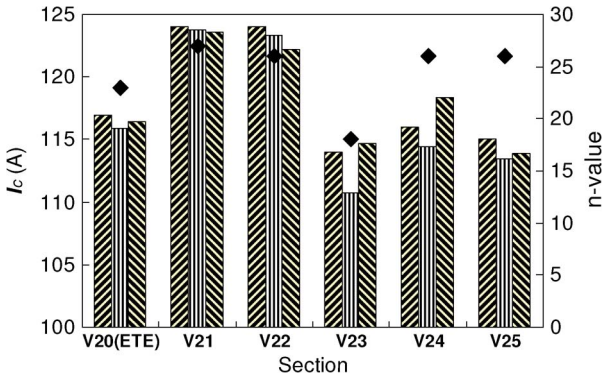

Fig. 2. Self-field I_c and n value at 77 K as a function of location on the sample. The vertical bars show results for the three repeated measurements. The diamonds indicate the average n value for the measurements.

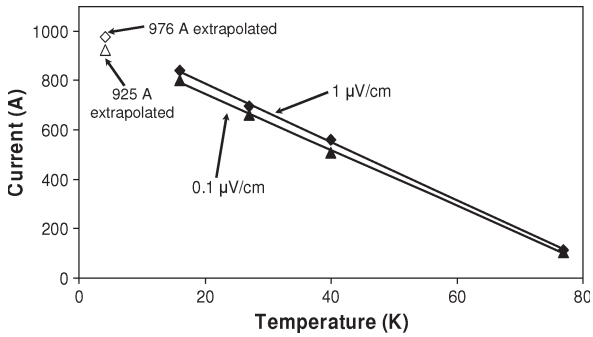

Fig. 3. I_c as a function of temperature using 1- and 0.1-μV/cm electric field criteria. The 77-K data are measured in liquid nitrogen, whereas the other measurements are measured during cooldown in helium. The points connected by the lines are the measured data, and the lines are fitting curves given in (1) and (2). The points at 4.2 K are extrapolated from these equations.

reduced I_c at the center section V23 is due to the Stycast that is used to ensure that the heater is mounted well; thus, there is no direct exposure to helium.

The ETE I_c's as a function of temperature are plotted in Fig. 3 for both a 1-μV/cm criterion and a 0.1-μV/cm criterion. The data are fit to linear expressions for each criterion [65], [66], i.e.,

$$I_c(T) = -11.85T + 1027.9 \text{ A} \quad (1\ \mu\text{V/cm criterion}) \qquad (1)$$

$$I_c(T) = -11.31T + 972.7 \text{ A} \quad (0.1\ \mu\text{V/cm criterion}). \qquad (2)$$

Equations (1) and (2) are extrapolated to 4.2 K, estimating $I_c(4.2\text{ K}, 1\ \mu\text{V/cm}) = 976.2$ A and $I_c(4.2\text{ K}, 0.1\ \mu\text{V/cm}) = 925.2$ A. Equations (1) and (2) are inverted to determine the current-sharing temperature $T_{\rm cs}$ as a function of I. These are plotted in Fig. 4, and the $T_{\rm cs}$ values for the values of I used in the quench measurements are summarized in Table I.

B. Transition From Recovery to Quench

Fig. 5 plots (a) voltage V23(t) and (b) temperature TC33(t) for a series of 300-ms heat pulses with increasing amplitude and a fixed $I = 350$ A. The temperature increases as soon as the heater pulse begins, whereas a measureable nonzero voltage appears hundreds of milliseconds later. When V23(t) becomes measurably nonzero, temperature TC33(t) has already reached

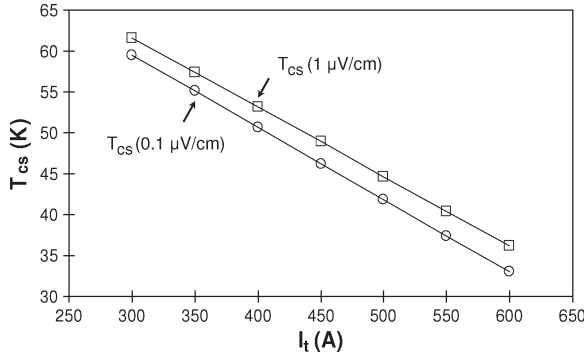

Fig. 4. Current-sharing temperature as a function of transport current using the results shown in Fig. 3.

TABLE I
DELAY TIMES BETWEEN THE BEGINNING OF THE HEAT PULSE AND THE ONSET OF A MEASURABLE NON ZERO VOLTAGE, AND UNTIL THE CURRENT-SHARING TEMPERATURE IS REACHED, AS A FUNCTION OF THE OPERATING CURRENT. TWO TIMES ARE GIVEN FOR THE TIME DELAY BEFORE REACHING THE CURRENT-SHARING TEMPERATURE BASED ON THE TWO ELECTRIC FIELD CRITERIA, AS SHOWN IN FIG. 4

Current (A)	Time (s) V24 > 0	TC34			
		Criterion: 1 μv/cm		Criterion: 0.1 μv/cm	
		T_{cs} (K)	δt (T_{cs}) (s)	T_{cs} (K)	δt (T_{cs}) (s)
550	0.20	40.4	0.543	37.4	0.533
500	0.25	44.7	0.653	41.8	0.633
450	0.26	48.9	0.783	46.2	0.763
400	0.24	53.1	1.103	50.7	1.073
350	0.24	57.4	1.203	55.1	1.093

100 K, which is much higher than $T_{\rm cs}$ (55 K–57 K), indicating that the measured surface temperature is higher than local temperature in the YBCO layer during the heater pulse. Note that the center thermocouple is embedded in the Stycast, where the heater is also attached, which contributes to the temperature gradient. The initial peaks in V23 and TC33, which occur just after the heat pulse ends, gradually increases with increasing heat pulse amplitudes. When the heater pulse voltage is 8.65 V, the maximum of V23(t) is less than 5 mV, although the input energy of 5.13 J is relatively high. Independent of the heater pulse energy (for the range used in this experiment), both V23 and TC33 decrease once the heat pulse ends, with the decrease in TC33 being rapid due to conduction along the length of the conductor and cooling by helium at the surface.

The transition from recovery to quench occurs when the heat pulse increased from 10.41 to 10.56 V. In this case, V23(t) linearly increases from $t = 0.72$ s to $t = 0.83$ s, indicative of current sharing from the YBCO to the stabilizer. It is unclear if, when V23(t) peaks at $t = 1.1$ s, the 350-A current is entirely redistributed to the stabilizer layers. This cannot be deduced from the temperature data because of the temperature gradient from the surface of the conductor to the YBCO layer. The V23(t) data are linear; however, with no change in slope, which may imply that current sharing is not complete, a change in slope is expected when the current is fully redistributed to the stabilizer, as the slope of V23(t) would mirror the temperature dependence of the resistivity of the Cu rather than the temperature

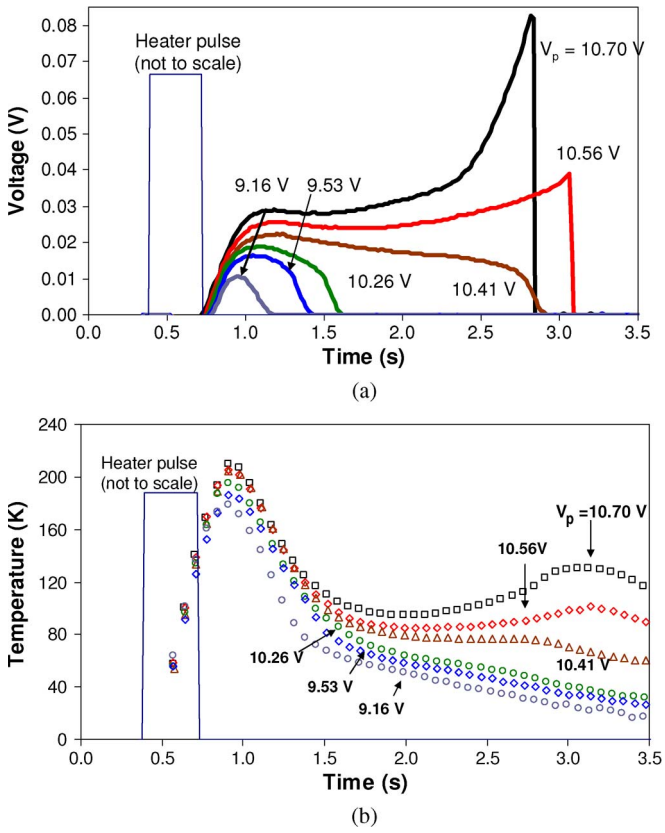

Fig. 5. (a) Voltage V23(t) and (b) temperature TC33(t) for a series of increasing heat pulse amplitudes with $I = 350$ A. The transition from recovery to quench is observed. The initial heat pulse causes a rapid spike in the temperature and voltage from which the conductor initially begins to recover from, even in the case of a quench. This is followed by a period of slowly increasing voltage and temperature as the current redistributes from the YBCO to the stabilizer and the resistive heating is greater than the surface cooling. Lastly, voltage and thermal runaway begin, and the experiment is terminated.

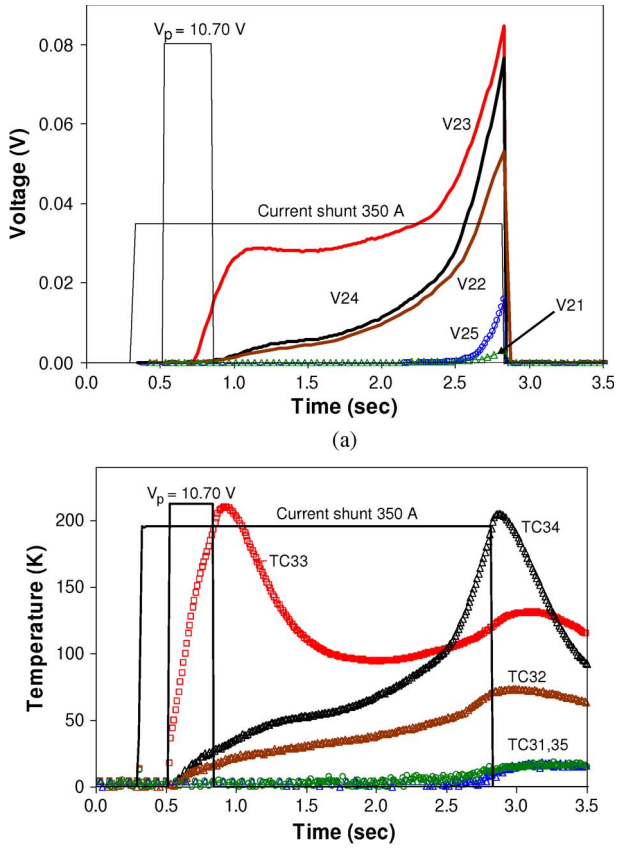

Fig. 6. (a) Voltages and (b) temperatures along the length of the YBCO CC during a quench with $I = 350$ A and $V_P = 10.70$ V, which is slightly above the MQE. Nonuniform propagation along the conductor length is observed.

dependence of I_c. During this period, the surface temperature rapidly increases to more than 200 K. After the heat pulse ends, V23(t) slowly decreases to 0.024 V at $t = 1.85$ s, whereas TC33(t) rapidly decreases to a local minimum of ~85 K. At this time, more than a full second after the heat pulse has ended, V23(t) and TC33(t) begin to slowly increase, indicating a quench. Thus, the resistive heating in the stabilizers due to current sharing is greater than the surface cooling from helium and conduction along the conductor. At $t = 3.01$ s, the transport current is turned off, because the ETE voltage reaches a set limit (300 mV). At this time, V23 = 39 mV. A few milliseconds later, at $t = 3.14$ s, TC33(t) peaks at 101 K. The results for a larger heater pulse amplitude, i.e., 10.70 V, are shown in Fig. 5. In this case, the same trends occur as in the 10.56-V case, but the second increase in V23(t) and TC33(t) more quickly begins after the heat pulse ends.

C. Voltage and Temperature Traces During a Quench

If the energy from the heater to the conductor exceeds the MQE, the normal zone propagates along the conductor, and nonzero voltages are measured in V22(t), V24(t), and possibly further along the conductor. Fig. 6 plots the (a) voltage and (b) temperature versus time for a quench with $I_t = 350$ A and heater pulse voltage = 10.70 V, which, as shown in Fig. 5, is ~1.5% above the MQE. The heat pulse begins at $t = 0.57$ s, and TC33(t) immediately increases while there is a delay in V23(t), which becomes nonzero at $t = 0.72$ s. TC32(t) and TC34(t), which are symmetrically located about TC33, simultaneously increase at $t = 0.71$ s, whereas V22(t) and V24(t) become measurably nonzero at $t = 0.75$ s. Note that the time lag between TC33(t) and V23(t) is much longer than that between TC34(t) and V24(t) and that the slopes of V23(t) and TC33(t) are much higher than the slopes of any other voltage or temperature traces. These differences are due to the rapid local heating due to the heater itself. At $t = 0.83$ s, although the pulse is off, V23(t) continues to increase and does not peak until $t = 1.01$ s. This is due to heat conduction normal to the conductor surface, where the temperature peaks at over 200 K, into to the YBCO layer, and is further evidence for a large temperature gradient in this direction. At $t = 2.58$ s, V21(t) and V25(t) become measurably nonzero due to normal zone propagation. In this case, there is a nearly simultaneous appearance of measurable nonzero voltages and an increase in the local temperature (TC31 and TC35). Moreover, before the transport current is terminated, TC32(t) and TC34(t) reach 75 and 200 K, respectively. The asymmetry between V22(t) and V24(t), and T32(t) and T34(t), results from inhomogeneities along the conductor length. Note also that TC34(t) is actually higher than TC33(t) for $t > 2.5$ s, which corresponds to the time at which V22(t)

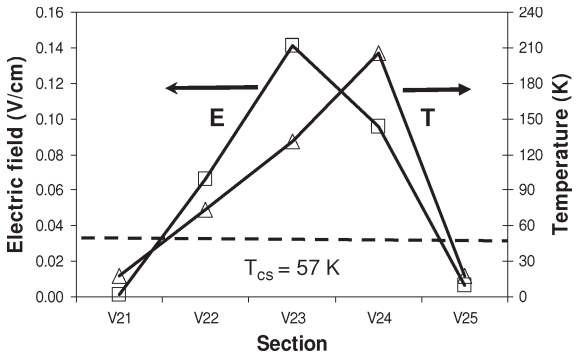

Fig. 7. Peak electric field and temperature along the length of the YBCO CC at the end of the quench shown in Fig. 6. The dashed line illustrates $T_{\rm cs}$ for this experiment.

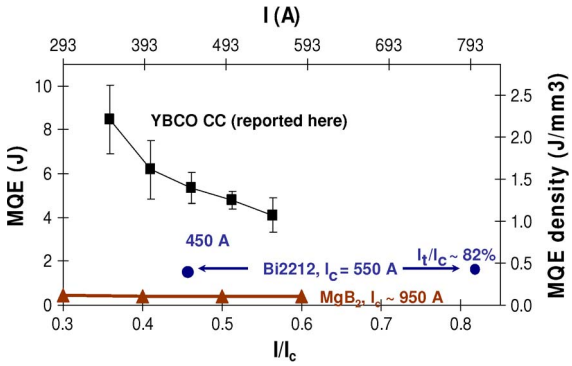

Fig. 8. MQE and MQE density versus I and I/I_c at 4.2 K for the YBCO CC studied here. Also shown are the MQE versus I and I/I_c at 4.2 K for $Bi_2Sr_2CaCu_2O_x$ (Bi2212) and MgB_2 round wires reported elsewhere [47], [52].

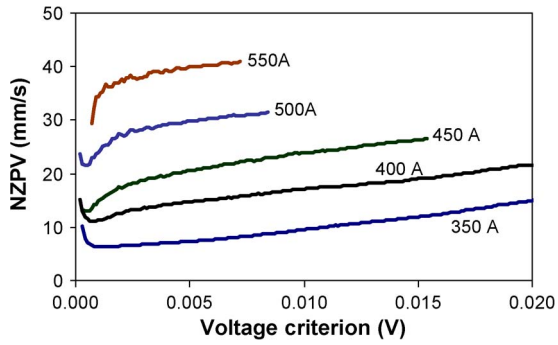

Fig. 9. NZPV versus voltage criterion for different transport currents.

and $V24(t)$ separate. This may be indicative of inhomogeneity in the Cu stabilizer or in the solder layer. Lastly, it is interesting that $TC31(t)$, $TC32(t)$, $TC33(t)$, and $TC35(t)$ continue to increase shortly after the transport current is terminated. This is due to heat conduction along the length of the conductor. Only $TC34(t)$, which is the hottest location at the end of the experiment, decreases as soon as the transport current ends.

The electric field and temperature peaks at the end of the 350-A quench (the data in Fig. 6) are plotted versus location in Fig. 7. (Note that the voltage data are converted to electric field to normalize out the varying tap distances.) The electric field data are for $t = 2.83$ s, and the temperature data are for $t = 3.07$ s. As expected, the center section has the largest electric field, but TC34 has a higher peak temperature than TC33. This is an artifact of the experimental geometry. The TC33 thermocouple is mounted atop the Stycast, whereas that of TC34 is directly attached to the conductor. Thus, TC33 is insulated from the heat source (resistive heating in the stabilizer), whereas TC34 is not, and the electric field profile is more indicative of the temperature within the YBCO for the center section of conductor. The time delay between the peak voltages and the peak temperatures is primarily because the hottest spot in the conductor is not at the surface, which is exposed to helium. The peak voltage occurs at the last measurement reading before turning off the transport current. The temperature slightly rises after that because of the temperature gradient normal to the conductor surface. The peak voltages or temperatures in V21 and V22 are below those of V24 and V25 due to inhomogeneities in the conductor. Although TC31 and TC35 are well below the current-sharing temperature ($\sim$57 K at $I = 350$ A, $E = 1$ μV/cm), V21 and V25 are measurably nonzero. This is due to the temperature gradient along the length of the conductor. TC31 and TC35 measure the temperature at the middle of sections V21 and V25. These sections are relatively long, i.e., 24 mm each, and the voltage is measuring the length-average electric field. Thus, there is a measurably nonzero voltage as soon as any portion of the 24-mm-long section across V21 or V25 has local temperature higher than $T_{\rm cs}$.

D. MQE

Fig. 5 shows that the MQE for $I = 350$ A corresponds to a heater pulse voltage of 10.56 V. The same procedure was repeated for I ranging from 400 to 550 A in 50-A intervals. At each current, the experiment was repeated, and the average MQE versus I is plotted in Fig. 8. The results are shown in terms of both MQE and MQE density in terms of I and I/I_c. As expected, MQE decreases as I increases. Consistent with other measurements of HTS quench behavior, the MQE values are very high, i.e., up to 9.0 J, which is higher than what is observed in LTS by about three orders of magnitude. These values likely overestimate the MQE, however, in that the ratio of the cooled surface to the conductor volume is very high, so the conductor is in a well-cooled geometry. Moreover, at low transport current, e.g., 350 or 400 A, not only is the MQE particularly large but the error bars that illustrate the spread in data for the repeated experiments shown in Fig. 8 are also large.

E. NZPV

To quantitatively characterize quench propagation, the NZPV is calculated using $V24(t)$ and $V25(t)$. Propagation distance $L_{\rm V24}$ is the length of V24, which slightly differs from how previous authors have defined it [48]–[50], because the voltage section lengths are different in this experiment. Here, NZPV is calculated using

$$\text{NZPV} = L_{\rm V24}/(t_{\rm V25} - t_{\rm V24}) \tag{3}$$

where $t_{\rm V25}$ and $t_{\rm V24}$ are the times when $V25(t)$ and $V24(t)$ reach a chosen voltage criterion. The calculated NZPV, as a function of voltage criterion and transport current, is plotted in Fig. 9. The propagation velocities at low voltage criteria show

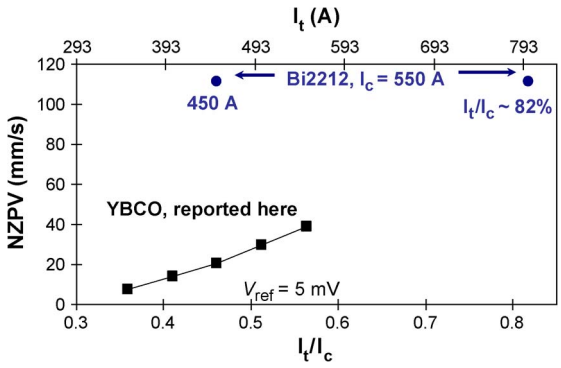

Fig. 10. NZPV for a voltage criterion of 5 mV versus I and I/I_c at 4.2 K for the YBCO CC studied here. Also shown is the NZPV versus I and I/I_c at 4.2 K for $Bi_2Sr_2CaCu_2O_x$ (Bi2212) round wires reported elsewhere [47].

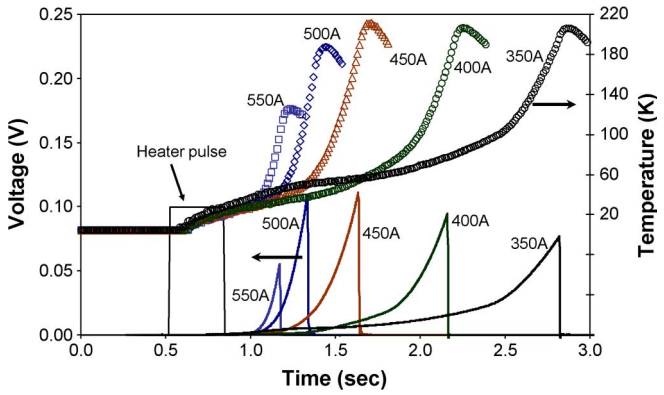

Fig. 11. $V24(t)$ and $TC34(t)$ as a function of transport current during quenches induced with quench energy slightly greater than the respective MQE.

an initial decrease with increasing criterion and vary by as much as 30%. This is most likely because, at the early stages of normal zone development, $V24(t)$ is influenced by both the heat pulse and the Joule heating, whereas $V25(t)$ is almost exclusively influenced by Joule heating. As the voltage criterion increases, so does the NZPV, and the dependence becomes linear for all currents, which is likely due to the temperature dependence of the stabilizer resistivity. Using a 5-mV criterion, NZPV versus I/I_c is plotted in Fig. 10. As seen with other HTS conductors, the dependence is linear.

IV. Discussion

A. Quench Onset and Implications for Quench Detection

The onset of quenching is more closely looked at in Figs. 11 and 12. Fig. 11 plots $V24(t)$ (lower curves) and $TC34(t)$ (upper curves) for I varying between 350 and 550 A, each with a quench energy slightly above the respective MQEs, and Fig. 12 plots the corresponding $V25(t)$ and $TC35(t)$. For the $TC34(t)$ data, there is an initial temperature rise that is relatively slow, during which time there is no measurable voltage increase (except for $I = 350$ A). This is due to the heater pulse being conducted along the stabilizer, which, other than the $I = 350$ A case (which required a very large heat pulse), does not significantly influence the YBCO layer. Shortly after the end of the heat pulse, the temperature and voltage then nearly simultaneously rise, indicating that the conductor is quenching, with the

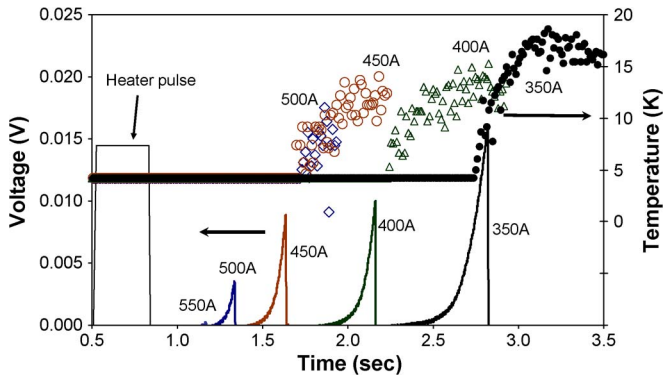

Fig. 12. $V25(t)$ and $TC35(t)$ as a function of transport current during quenches induced with quench energy slightly greater than the respective MQE. No measurable temperature is observed when the transport current is 550 A. The temperatures in the case of (open diamond) 500 A, (open circle) for 450 A, (open triangle) 400 A, and (closed circle) 350 A are shown.

delay time between the end of the heat pulse and the onset of the thermal and voltage runaway decreasing as I increases. The decreasing delay time indicates that the transition is driven by the resistive heating in the stabilizer, which increases with I, rather than the heat pulse, which decreases with I. In the 350- and 400-A cases, the transition is slow with a drawn-out current-sharing time (the extended period with a relatively low slope in both the voltage and temperature curves). This is quantified in Table I, which lists $T_{cs}(I)$ for each current value studied along with the delay times $t(T_{cs})$, which are defined as the time delay from the start of the heater pulse (the equivalent of the beginning of a disturbance in a magnet) until the current-sharing temperature is reached, where the current-sharing temperatures for the two electric field criteria are from Fig. 4. These values illustrate the slow dynamics of quench nucleation in YBCO conductors.

Fig. 12 shows that, as with $V24(t)$ and $T34(t)$, there is a distinct time delay between the onset of a measurable nonzero voltage and the increase in temperature for $V25(t)$ and $T35(t)$. At this location, because there is no effect of the heat pulse on the voltage or temperature, only the effects of quench propagation are observed. Unlike $T34(t)$, the initial slope of $T35(t)$ is sharp, indicating that the primary heat source is the Joule heating and not thermal conduction from the neighboring section. The time delay between $V25(t)$ and $T35(t)$ is, again, an artifact of both temperature gradients. The horizontal temperature gradient results in an electric field within the voltage taps that produce $V25(t)$, whereas the normal gradient results in higher temperature at the YBCO layer than at the surface. Thus, while this section of the CC may have significant or even complete current sharing, the helium at the surface delays the increase in $T35(t)$.

Due to the slow quench propagation, one of the challenges for quench protection is quench detection. One concept that is being considered is to use fiber-optic quench detection, because it can provide more detailed spatial information than voltage measurements, which are length averages, with a fast response time [67]. The fiber-optic sensors, however, are based on detecting changes in temperature. Thus, if a significant thermal gradient exists between the YBCO layer and the CC surface,

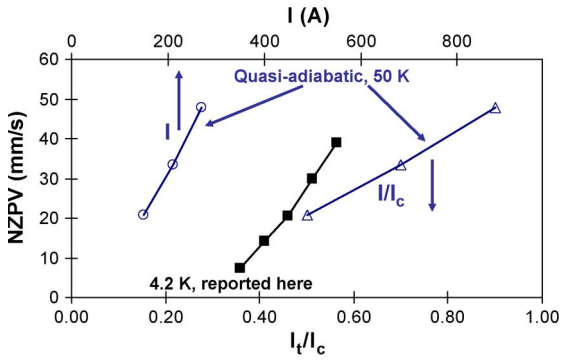

Fig. 13. NZPV data from Fig. 10 for the YBCO reported here compared to NZPV data for a YBCO CC measured at 50 K in a quasi-adiabatic environment [50].

then a surface-temperature-based quench detection system must take into account that the internal temperature, which is most critical to preventing permanent damage, is higher than that measured on the surface.

B. Comparison With Other Emerging Superconducting Conductors

Figs. 8 and 10 compare the YBCO CC MQE and NZPV results obtained here with data reported elsewhere for $Bi_2Sr_2CaCu_2O_x$ (Bi2212) and MgB_2 round wires at 4.2 K with a similar experimental setup [47], [52]. Comparing to Bi2212, it is important to first note that the I_c(Bi2212) reported is only 550 A. Interestingly, however, when plotted versus I/I_c, the MQE and the NZPV of YBCO appear to extrapolate to the Bi2212 results. When compared to the fixed values obtained at $I = 450$ A, however, the YBCO CC is much more stable with $\sim$2.5 times greater MQE and a factor-of-over-five slower propagation. This is clearly due to the difference in I/I_c for the fixed I and, thus, the presumably much lower T_{cs} for the Bi2212 (not reported). Comparing to the MgB_2 wire, which has I_c similar to that of the YBCO but much lower T_c, the YBCO is significantly more stable, with MQE ranging from five to ten times higher. Similarly, the MgB_2 wire has an NZPV that is about 20 times faster than that of the YBCO. (This is not plotted because the difference is too large for the scale range.) Thus, of the emerging conductors with potential for application at 4.2 K, YBCO CCs are the most stable but also the most challenging for quench detection.

C. Comparison With YBCO CC at Higher Temperature

Fig. 13 replots the YBCO CC data shown in Fig. 10 and compares it to previously reported data for YBCO CC at 50 K [50]. In the comparison case, the YBCO CC was cooled by a cryocooler in a vacuum and was thus quasi-adiabatic. When comparing on a fixed-current basis, the NZPV is much faster at 50 K, although I_c is much lower, than that at 4.2 K because of the absence of direct liquid or gas cooling to the surface. For a fixed I/I_c, the NZPV at 4.2 K is significantly higher for the range of I/I_c for which the data sets overlap. Due to the difference in slope, it is unclear if the 50-K adiabatic case would have higher NZPV at lower fraction of I/I_c.

V. Conclusion

The stability and quench behavior of YBCO CC at 4.2-K self-field has been investigated over a range of transport current. The conductor is very stable and has very slow NZPV. Due to the temperature gradient along the conductor length and normal to the surface, the onset of a measurably nonzero voltage occurs before the surface temperature reaches the current-sharing temperature. This may have implications for the development of quench protection in YBCO magnets.

The MQE of YBCO CC at 4.2 K is approximately three orders of magnitude greater than that of LTS conductors and, for the parameter ranges studied here, significantly more stable than MgB_2. Compared to Bi2212, the fundamental behavior is very similar, and the stability and quench behavior is, thus, driven by the specifics of the conductor geometry and, in particular, conductor I_c.

Acknowledgment

The authors would like to thank C. Thieme of the American Superconductor Corporation for the 344 YBCO coated conductor used in this study and U. P. Trociewitz, X. Wang, and T. Effio for the assistance and useful discussions.

References

[1] K. Ohkura, K. Sato, M. Ueyama, J. Fujikami, and Y. Iwasa, "Generation of 24.0 T at 4.2 K and 23.4 T at 27 K with a high-temperature superconductor coil in a 22.54 T background field," *Appl. Phys. Lett.*, vol. 67, no. 13, pp. 1923–1925, Sep. 1995.

[2] H. W. Weijers, U. P. Trociewitz, K. Marken, M. Meinesz, H. Miao, and J. Schwartz, "The generation of 25.05 T using a 5.11 $TBi_2Sr_2CaCu_2O_x$ superconducting insert magnet," *Supercond. Sci. Technol.*, vol. 17, no. 4, pp. 636–644, Apr. 2004.

[3] J. Schwartz, T. Effio, X. Liu, Q. V. Le, A. L. Mbaruku, H. J. Schneider-Muntau, T. Shen, H. Song, U. P. Trociewitz, X. Wang, and H. W. Weijers, "High field superconducting solenoids via high temperature superconductors," *IEEE Trans. Appl. Supercond.*, vol. 18, no. 2, pp. 70–81, Jun. 2008.

[4] J. Clarke and D. C. Larbalestier, "Wired for the future," *Nat. Phys.*, vol. 2, no. 12, pp. 794–796, Dec. 2006.

[5] R. M. Scanlan, A. P. Malozemoff, and D. C. Larbalestier, "Superconducting materials for large scale applications," *Proc. IEEE*, vol. 92, no. 10, pp. 1639–1654, Oct. 2004.

[6] J. L. Macmanus-Driscoll, S. R. Foltyn, Q. X. Jia, H. Wang, A. Serquis, L. Civale, B. Maiorov, M. E. Hawley, M. P. Maley, and D. E. Peterson, "Strongly enhanced current densities in superconducting coated conductors of YBa2Cu3O7-x+BaZrO3," *Nat. Mater.*, vol. 3, no. 7, pp. 439–443, Jul. 2004.

[7] D. Larbalestier, A. Gurevich, D. M. Feldmann, and A. Polyanskii, "High-T-c superconducting materials for electric power applications," *Nature*, vol. 414, no. 6861, pp. 368–377, Nov. 2001.

[8] T. Haugan, P. N. Barnes, R. Wheeler, F. Meisenkothen, and M. Sumption, "Addition of nanoparticle dispersions to enhance flux pinning of the YBa2Cu3O7-x superconductor," *Nature*, vol. 430, no. 7002, pp. 867–870, Aug. 2004.

[9] C. V. Varanasi, J. Burke, H. Wang, J. H. Lee, and P. N. Barnes, "Thick YBa2Cu3O7-x+BaSnO3 films with enhanced critical current density at high magnetic fields," *Appl. Phys. Lett.*, vol. 93, no. 9, pp. 092 501-1–092 501-3, Sep. 2008.

[10] S. Kang, A. Goyal, J. Li, A. A. Gapud, P. M. Martin, L. Heatherly, J. R. Thompson, D. K. Christen, F. A. List, M. Paranthaman, and D. F. Lee, "High-performance high-T-c superconducting wires," *Science*, vol. 311, no. 5769, pp. 1911–1914, Mar. 2006.

[11] T. Aytug, M. Paranthaman, K. J. Leonard, K. Kim, A. O. Ijaduola, Y. Zhang, E. Tuncer, J. R. Thompson, and D. K. Christen, "Enhanced flux pinning and critical currents in YBa2Cu3O7-delta films by nanoparticle surface decoration: Extension to coated conductor templates," *J. Appl. Phys.*, vol. 104, no. 4, pp. 043 906-1–043 906-6, Aug. 2008.

[12] A. Goyal, J. Li, P. M. Martin, A. Gapud, E. Specht, M. Paranthaman, X. Li, W. Zhang, T. Kodenkandath, and M. Rupich, "Enhanced flux-pinning in dy-doped, MOD YBCO films on RABiTS," *IEEE Trans. Appl. Supercond.*, vol. 17, no. 2, pp. 3340–3342, Jun. 2007.

[13] T. G. Holesinger, B. Maiorov, J. Y. Coulter, L. Civale, X. Li, W. Zhang, Y. Huang, T. Kodenkandath, and M. W. Rupich, "Key microstructural features of MOD YBa2Cu3O7-partial derivative films on textured nickel substrates," *IEEE Trans. Appl. Supercond.*, vol. 17, no. 2, pp. 3259–3262, Jun. 2007.

[14] X. Li, M. W. Rupich, T. Kodenkandath, Y. Huang, W. Zhang, E. Siegal, D. T. Verebelyi, U. Schoop, N. Nguyen, C. Thieme, Z. Chen, D. M. Feldman, D. C. Larbalestier, T. G. Holesinger, L. Civale, Q. X. Jia, V. Maroni, and M. V. Rane, "High critical current YBCO films prepared by an MOD process on RABiTS templates," *IEEE Trans. Appl. Supercond.*, vol. 17, no. 2, pp. 3553–3556, Jun. 2007.

[15] M. P. Paranthaman, S. Sathyamurthy, M. S. Bhuiyan, P. M. Martin, T. Aytug, K. Kim, M. Fayek, K. J. Leonard, J. Li, A. Goyal, T. Kodenkandath, X. Li, W. Zhang, and M. W. Rupich, "MOD Buffer/YBCO approach to fabricate low-cost second generation HTS wires," *IEEE Trans. Appl. Supercond.*, vol. 17, no. 2, pp. 3332–3335, Jun. 2007.

[16] N. M. Strickland, N. J. Long, J. Xia, J. Kennedy, A. Markwitz, A. Zondervan, M. W. Rupich, W. Zhang, X. Li, T. Kodenkandath, and Y. Huang, "Enhanced flux pinning in MOD second generation HTS wires by silver- and copper-ion irradiation," *IEEE Trans. Appl. Supercond.*, vol. 17, no. 2, pp. 3306–3309, Jun. 2007.

[17] W. Zhang, Y. Huang, X. Li, T. Kodenkandath, M. W. Rupich, U. Schoop, D. T. Verebelyi, C. L. H. Thieme, E. Siegal, T. G. Holesinger, B. Maiorov, L. Civale, D. J. Miller, V. A. Maroni, J. Li, P. M. Martin, E. D. Specht, A. Goyal, and M. P. Paranthaman, "Control of flux pinning in MOD YBCO coated conductor," *IEEE Trans. Appl. Supercond.*, vol. 17, no. 2, pp. 3347–3350, Jun. 2007.

[18] X. Y. Song, Z. J. Chen, S. I. Kim, M. Feldmann, D. Larbalestier, J. Reeves, Y. Xie, and V. Selvamanickam, "Evidence for strong flux pinning by small, dense nanoprecipitates in a Sm-doped YBa2Cu3O7-delta coated conductor," *Appl. Phys. Lett.*, vol. 88, no. 21, p. 212 508, May 2006.

[19] Y. L. Zuev, D. K. Christen, S. H. Wee, A. Goyal, and S. W. Cook, "Near-isotropic performance of intrinsically anisotropic high-temperature superconducting tapes due to self-assembled nanostructures," *Appl. Phys. Lett.*, vol. 93, no. 17, p. 172 512, Oct. 2008.

[20] S. H. Wee, A. Goyal, J. Li, Y. L. Zuev, S. Cook, and L. Heatherly, "The incorporation of nanoscale columnar defects comprised of self-assembled BaZrO3 nanodots to improve the flux pinning and critical current density of NdBa2Cu3O7-delta films grown on RABiTS," *Supercond. Sci. Technol.*, vol. 20, no. 8, pp. 789–793, Aug. 2007.

[21] S. H. Wee, A. Goyal, P. M. Martin, and L. Heatherly, "High in-field critical current densities in epitaxial NdBa2Cu3O7-delta films on RABiTS by pulsed laser deposition," *Supercond. Sci. Technol.*, vol. 19, no. 8, pp. 865–868, Aug. 2006.

[22] S. H. Wee, A. Goyal, Y. L. Zuev, and C. Cantonil, "High performance superconducting wire in high applied magnetic fields via nanoscale defect engineering," *Supercond. Sci. Technol.*, vol. 21, no. 9, p. 092 001, Sep. 2008.

[23] S. I. Kim, F. Kametani, Z. Chen, A. Gurevich, D. C. Larbalestier, T. Haugan, and P. Barnes, "On the through-thickness critical current density of an YBa2Cu3O7-x film containing a high density of insulating, vortex-pinning nanoprecipitates," *Appl. Phys. Lett.*, vol. 90, no. 25, p. 252 502, Jun. 2007.

[24] C. L. H. Thieme, K. J. Gagnon, J. Y. Coulter, H. Song, and J. Schwartz, "Stability of second generation HTS pancake coils at 4.2 K for high heat flux applications," *IEEE Trans. Appl. Supercond.*, vol. 19, no. 3, Jun. 2009.

[25] D. Uglietti, B. Seeber, V. Abacherli, W. L. Carter, and R. Flükiger, "Critical currents versus applied strain for industrial Y-123 coated conductors at various temperatures and magnetic fields up to 19 T," *Supercond. Sci. Technol.*, vol. 19, no. 8, pp. 869–872, Aug. 2006.

[26] D. W. Hazelton, V. Selvamanickam, and J. M. Duval, "Recent development in 2G HTS coil technology," *IEEE Trans. Appl. Supercond.*, vol. 19, no. 3, pt. 2, Jun. 2009.

[27] A. P. Malozemoff, S. Fleshler, M. Rupich, C. Thieme, X. Li, W. Zhang, A. Otto, J. Maguire, D. Folts, J. Yuan, H.-P. Kraemer, W. Schmidt, M. Wohlfart, and H.-W. Neumueller, "Progress in high temperature superconductor coated conductors and their applications," *Supercond. Sci. Technol.*, vol. 21, no. 3, p. 034 005, 2008.

[28] V. V. Kashikhin, E. Barzi, V. S. Kashikhin, M. Lamm, Y. Sadovskiy, and A. V. Zlobin, "Study of high field superconducting solenoids for Muon beam cooling," *IEEE Trans. Appl. Supercond.*, vol. 18, no. 2, pp. 928–932, Jun. 2008.

[29] W. D. Markiewicz, J. R. Miller, J. Schwartz, U. P. Trociewitz, and H. W. Weijers, "Perspective on a superconducting 30 T/1.3 GHz NMR spectrometer magnet," *IEEE Trans. Appl. Supercond.*, vol. 16, no. 2, pp. 1523–1526, Jun. 2006.

[30] T. Ando, S. Nishio, and H. Yoshimura, "Design of the high-T-c superconducting TF coil for the tight aspect ratio tokamak power reactor (VECTOR)," *IEEE Trans. Appl. Supercond.*, vol. 14, no. 2, pp. 1481–1484, Jun. 2004.

[31] P. J. Masson, V. R. Rouault, G. Hoffmann, and C. A. Luongo, "Development of quench propagation models for coated conductors," *IEEE Trans. Appl. Supercond.*, vol. 18, no. 2, pp. 1321–1324, Jun. 2008.

[32] V. Sokolovsky and V. Meerovich, "Normal zone propagation along superconducting films deposited on wide substrates," *Cryogenics*, vol. 48, no. 9/10, pp. 397–405, Sep./Oct. 2008.

[33] C. E. Oberly, "Improved dielectric material for passive quench protection of superconductor operating near 77 K," in *Proc. CHATS*, Berkeley, CA, Sep. 5–7, 2006. [Online]. Available: http://www.supercon.lbl.gov/chats/Talks/Wednesday_morning/CEOberly.ppt

[34] R. Grabovickic, J. W. Lue, M. J. Gouge, J. A. Demko, and R. C. Duckworth, "Measurements of temperature dependence of the stability and quench propagation of a 20-cm-long RABiTS Y-Ba-Cu-O tape," *IEEE Trans. Appl. Supercond.*, vol. 13, no. 2, pp. 1726–1730, Jun. 2003.

[35] A. Ishiyama, M. Yanai, T. Morisaki, H. Ueda, Y. Shiohara, T. Izumi, Y. Iijima, and T. Saitoh, "Normal transition and propagation characteristics of YBCO tape," *IEEE Trans. Appl. Supercond.*, vol. 15, no. 2, pp. 1659–1662, Jun. 2005.

[36] R. C. Duckworth, J. W. Lue, D. E. Lee, R. Grabovickic, and M. J. Gouge, "The role of nickel substrates in the quench dynamics of silver coated YBCO tapes," *IEEE Trans. Appl. Supercond.*, vol. 13, no. 2, pp. 1768–1771, Jun. 2003.

[37] S.-C. Kim, D.-W. Ha, S.-S. Oh, I.-Y. Han, J.-G. Oh, and H.-S. Sohn, "Effect of filament configuration on critical current density of Bi2212/Ag wires with low Ag ratio," *IEEE Trans. Appl. Supercond.*, vol. 18, no. 2, pp. 1188–1191, Jun. 2008.

[38] W. S. Kim, F. Trillaud, M. C. Ahn, Y. Iwasa, X. Peng, and M. Tomsic, "Normal zone propagation in 2-dimensional YBCO winding pack models," *IEEE Trans. Appl. Supercond.*, vol. 18, no. 2, pp. 1249–1252, Jun. 2008.

[39] W. S. Kim, F. Trillaud, M. C. Ahn, Y. Iwasa, X. Peng, and M. Tomsic, "Detect-and-activate-the-heater protection technique for YBCO coils," *IEEE Trans. Appl. Supercond.*, vol. 18, no. 2, pp. 1337–1340, Jun. 2008.

[40] W. S. Kim, F. Trillaud, I. C. Ang, S.-Y. Hahn, and Y. Iwasa, "Normal zone propagation in YBCO winding pack models," *IEEE Trans. Appl. Supercond.*, vol. 17, no. 2, pp. 2478–2481, Jun. 2007.

[41] M. Breschi, P. L. Ribani, X. Wang, and J. Schwartz, "Theoretical explanation of the non-equipotential quench behaviour in Y-Ba-Cu-O coated conductors," *Supercond. Sci. Technol.—Rapid Commun.*, vol. 20, no. 4, pp. L9–L11, Apr. 2007.

[42] G. A. Levin and P. N. Barnes, "The normal zone in YBa2Cu3O6+x-coated conductors," *Supercond. Sci. Technol.*, vol. 20, no. 12, pp. 1101–1107, Dec. 2007.

[43] G. A. Levin, P. N. Barnes, and J. S. Bulmer, "Current sharing between superconducting film and normal metal," *Supercond. Sci. Technol.*, vol. 20, no. 8, pp. 757–764, Aug. 2007.

[44] F. Trillaud, M. C. Ahn, J. Bascunan, W.-S. Kim, J. P. Voccio, and Y. Iwasa, "Quench behavior, quench protection of a YBCO test coil assembly," *IEEE Trans. Appl. Supercond.*, vol. 18, no. 2, pp. 1329–1332, Jun. 2008.

[45] F. Trillaud, I. C. Ang, W. S. Kim, H. G. Lee, Y. Iwasa, and J. P. Voccio, "Protection and quench detection of YBCO coils results with small test coil assemblies," *IEEE Trans. Appl. Supercond.*, vol. 17, no. 2, pp. 2450–2453, Jun. 2007.

[46] T. Effio, U. P. Trociewitz, X. Wang, and J. Schwartz, "Quench induced degradation in Bi2Sr2CaCu2O8+x tape conductors at 4.2 K," *Supercond. Sci. Technol.*, vol. 21, no. 4, p. 045 101, Apr. 2008.

[47] J. Schwartz, T. Effio, U. P. Trociewitz, and X. R. Wang, "Quench induced degradation in $Bi_2Sr_2CaCu_2O_x$ round wires and coils at 4.2 K," *J. Appl. Phys.*, 2009, submitted for publication.

[48] F. Trillaud, H. Palanki, U. P. Trociewitz, S. H. Thompson, H. W. Weijers, and J. Schwartz, "Normal zone propagation experiments on HTS composite conductors," *Cryogenics*, vol. 43, no. 3–5, pp. 271–279, Mar.–May 2003.

[49] U. P. Trociewitz, B. Czabaj, S. Hong, Y. Huang, D. C. Knoll, D. C. Larbalestier, W. D. Markiewicz, H. Miao, M. Meinesz, X. Wang, and J. Schwartz, "Quench studies on a layer-wound $Bi_2Sr_2CaCu_2Ox$/AgX coil at 4.2 K," *Supercond. Sci. Technol.*, vol. 21, no. 2, p. 025 015, Feb. 2008.

[50] X. Wang, U. P. Trociewitz, and J. Schwartz, "Near-adiabatic quench experiments on short$YBa_2Cu_3O_{7-\delta}$ coated conductors," *J. Appl. Phys.*, vol. 101, no. 5, p. 053 904, Mar. 2007.

[51] X. R. Wang, A. R. Caruso, M. Breschi, G. Zhang, U. P. Trociewitz, H. W. Weijers, and J. Schwartz, "Normal zone initiation and propagation in Y-Ba-Cu-O coated conductors with Cu stabilizer," *IEEE Trans. Appl. Supercond.*, vol. 15, no. 2, pp. 2586–2589, Jun. 2005.

[52] X. R. Wang, S. V. P. S. S. Pamidi, U. P. Trociewitz, and J. Schwartz, "Self-field quench behavior of multifilamentaryMgB_2 wires in liquid helium," *Cryogenics*, vol. 48, no. 11/12, pp. 469–477, Nov./Dec. 2008.

[53] A. L. Mbaruku, U. P. Trociewitz, X. Wang, and J. Schwartz, "Relationships between conductor damage, quenching and electromechanical behavior in YBCO coated conductors," *IEEE Trans. Appl. Supercond.*, vol. 17, no. 2, pp. 3044–3049, Jun. 2007.

[54] G. M. Zhang, D. J. Knoll, D. N. Nguyen, P. V. P. S. S. Sastry, X. Wang, and J. Schwartz, "Quench behavior of YBa2Cu3O7 coated conductor with AC transport current," *IEEE Trans. Appl. Supercond.*, vol. 17, no. 4, pp. 3874–3879, Dec. 2007.

[55] A. L. Rakhmanov, V. S. Vysotsky, Y. A. Ilyin, T. Kiss, and M. Takeo, "Universal scaling law for quench development in HTSC devices," *Cryogenics*, vol. 40, no. 1, pp. 19–27, Jan. 2000.

[56] V. S. Vysotsky, Y. A. Ilyin, T. Kiss, M. Inoue, M. Takeo, F. Irie, H. Okamoto, M. Kanazawa, K. Ohya, S. Hayashida, and A. L. Rakhmanov, "Thermal quench study in HTSC pancake coil," *Cryogenics*, vol. 40, no. 1, pp. 9–17, Jan. 2000.

[57] Y. A. Ilyin, V. S. Vysotsky, T. Kiss, M. Takeo, H. Okamoto, and F. Irie, "Stability and quench development study in small HTSC magnet," *Cryogenics*, vol. 41, no. 9, pp. 665–674, Sep. 2001.

[58] J. Voccio, C. King, D. Aized, C. Thieme, T. MacDonald, G. Snitchler, B. Gamble, and A. P. Malozemoff, "2G HTS wires and the implications for motor and generator applications," *IEEE Trans. Appl. Supercond.*, vol. 17, no. 2, pp. 1591–1594, Jun. 2007.

[59] S. D. Umans, B. A. Shoykhet, J. K. Zevchek, C. M. Rey, and R. C. Duckworth, "Quench in high-temperature superconducting motor field coils: Experimental results at 30 K," *IEEE Trans. Appl. Supercond.*, vol. 17, no. 2, pp. 1561–1567, Jun. 2007.

[60] L. Li, T. Zhang, W. Wang, J. Alexander, X. Huang, K. Sivasubramaniam, E. T. Laskaris, J. W. Bray, and J. M. Fogarty, "Quench test of HTS coils for generator application at GE," *IEEE Trans. Appl. Supercond.*, vol. 17, no. 2, pp. 1575–1578, Jun. 2007.

[61] W. S. Wang, L. Li, T. Zhang, J. P. Alexander, X. Huang, E. T. Laskaris, J. W. Bray, and J. M. Fogarty, "Overcurrent simulation test for high-temperature superconducting generator," *IEEE Trans. Ind. Appl.*, vol. 44, no. 4, pp. 1160–1164, Jul./Aug. 2008.

[62] W. D. Markiewicz, "Protection of HTS coils in the limit of zero quench propagation velocity," *IEEE Trans. Appl. Supercond.*, vol. 18, no. 2, pp. 1333–1336, Jun. 2008.

[63] X. Li *et al.*, "The development of second generation HTS wire at American Superconductor," *IEEE Trans. Appl. Supercond.*, vol. 19, no. 3, pt. 3, Jun. 2009.

[64] J. W. Ekin, *Experimental Techniques for Low Temperature Measurements*. London, U.K.: Oxford Univ. Press, 2006, pp. 324–328.

[65] Y. Iwasa, *Case Studies in Superconducting Magnets*. New York: Springer-Verlag, 1994.

[66] M. N. Wilson, *Superconducting Magnets*. Oxford, U.K.: Clarendon Press, 1983, pp. 76–97.

[67] J. Schwartz, R. P. Johnson, and S. A. Kahn, "Multi-purpose fiber optic sensors for HTS magnets," in *Proc. 11th Eur. Particle Accelerator Conf.*, Genoa, Italy, 2008.

Honghai Song (S'08) received the B.S. and M.S. degrees in electrical engineering from Southwest Jiaotong University, Chengdu, China, in 2001 and 2004, respectively. He is currently working toward the Ph.D. degree in the Applied Superconductivity Center, National High Magnetic Field Laboratory, and the Department of Electrical and Computer Engineering, FAMU-FSU College of Engineering, Florida State University, Tallahassee.

His research interests include stability and quench of high-temperature superconductor with electromagnetic characterization and cryogenic instrumentation, focusing on the dynamic observation of normal zone propagation in a Y-Ba-Cu-O coated conductor using magnetooptical imaging and microstructure analysis.

Justin Schwartz (M'91–SM'01–F'04) received the Ph.D. degree in nuclear engineering from Massachusetts Institute of Technology, Cambridge, in 1990.

He is currently the Jack E. Crow Professor of Engineering with the Applied Superconductivity Center, National High Magnetic Field Laboratory, and the Department of Mechanical Engineering, FAMU-FSU College of Engineering, Florida State University, Tallahassee. His research interests include the science and engineering of high-temperature superconductors for applications.